

# Mott insulator phases of non-locally coupled bosons in bilayer optical superlattices

Sayan Lahiri<sup>1</sup>, Suman Mondal<sup>1</sup>, Manpreet Singh<sup>1</sup> and Tapan Mishra<sup>1</sup>  
<sup>1</sup>*Department of Physics, Indian Institute of Technology, Guwahati-781039, India*  
 (Dated: February 18, 2022)

We investigate the ground state properties of a non-locally coupled bosonic system in a bilayer optical superlattice by considering bosons in one layer to be of softcore in nature and separately allowing two and three body hardcore constraints on the other layer. We find that the presence of different constraints on bosons in one layer influences the overall phase diagram exhibiting various Mott insulator phases at incommensurate densities due to the presence of the superlattice potential apart from the usual Mott insulators at commensurate densities. Moreover, the presence of two or three-body constraints significantly modifies the Mott insulator-Superfluid phase transition points as a function of the superlattice potential. Due to the various competing interactions, constraints and superlattice potential the phase diagrams exhibit significantly different features. We obtain the complete phase diagrams by using the cluster-mean-field theory approach. We further extend this work to a coupled two-leg ladder superlattice where we obtain similar physics using the density matrix renormalization group method .

## I. INTRODUCTION

Quantum phase transitions in systems of ultracold quantum gases in optical lattices have revealed a host of new phenomena in recent years. The rapid progress in experimental manipulation of these weakly interacting systems in optical lattices has allowed to uncover various interesting physics which were impossible to understand using the conventional solid state systems. One such example is the observation of the superfluid (SF) to Mott insulator (MI) phase transition in a three-dimensional optical lattice [1], the phenomenon which was predicted in the context of the Bose-Hubbard model [2, 3]. The state-of-the-art experimental set ups and the flexibility to control the system parameters in such systems have provided a new platform to explore interesting phenomena in nature which has led to a plethora of novel and exciting physics. While the dominant interaction in such ultracold systems is the two-body contact interactions, it has been shown that there exist higher order local interactions as well, which have non-negligible effects on the ground state properties [4, 5]. Recently it was shown that the leading multi-body interactions, such as the three-body interaction, can be engineered under suitable conditions in optical lattices [6–9] which can play important roles in discovering many-body induced quantum phases, especially at higher densities [10, 11]. Such many-body interactions can drastically modify the behaviour of the system. For instance, the three-body interaction can become very large leading to the three-body hardcore constrained where not more than two particles can occupy a single site. This feature is crucial in studying the systems of attractive bosons in optical lattices by preventing the collapse of bosons. These three-body constrained bosons (TBCs) are shown to exhibit the superfluid to pair-superfluid (PSF) phase transition in optical lattice [12]. Similar situation is also seen in the regime of large onsite two-body repulsion where no two bosons can simultaneously occupy a single site. In such a situation the bosons are called the hardcore bosons (HCBs) or the

Tonk's gas [13].

On the other hand long-range dipolar interactions in atoms, molecules and Rydberg atoms have culminated into a completely new realm of physics where several novel phenomena have been predicted and observed in recent experiments such as the CDW phases, the exotic supersolid phases and self-bound quantum droplets [14–18]. Interestingly, these non-local interactions have shown to couple systems which are spatially separated from each other such as the bilayer systems and two leg ladders. In such a scenario one can drive the two decoupled systems together with the help of the long-range dipole-dipole interaction [19–22]. Moreover, the bilayer systems with inter-layer interactions resemble systems of two component atomic mixtures in optical lattices. A new area of research has evolved in the context of the dual species bosons, fermions as well as Bose-Fermi mixtures due to the recent advancement in cooling and trapping of binary mixtures in experiments [23–32]. The creation and manipulation of such dual-species mixtures with completely two different species of atoms or two hyperfine states of a particular species in optical lattices to achieve strong correlations have opened up various avenues in addressing complex many-body systems. The presence of different types of interactions compared to the single species systems have made the binary mixture a topic of great interest, as a result several theoretical predictions and experimental observations have been made in various context [28, 30–43]. At the same time the creation of optical superlattices [44, 45] have proven to provide an additional flexibility to manipulate lattice potentials and periodicity which results in different interesting applications. A great deal of research has been done on optical superlattices and several new phases have been predicted in theory and observed in experiments on various context [44, 46–57]. Although various investigations have been made in systems of ultracold quantum gases in optical superlattices, the study of bilayer superlattice or binary mixture in superlattices may lead to novel phenomena. As the systems of dual species mixture can be

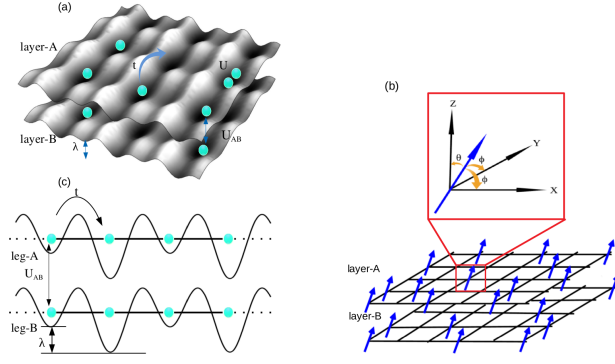


FIG. 1. (Color online)(a) Illustration of a bilayer superlattice having periodicity equal to two showing the intra-layer and inter-layer interactions. (b) The possible alignment of the dipoles in this bilayer system. In the inset we have shown one dipole placed in the origin in such a way that it makes an angle  $\phi$  with the  $x$  and  $y$  axes and  $\theta$  with the  $z$  axis. (c) Two leg optical superlattice with leg-A and leg-B containing the soft-core bosons and constrained bosons respectively. These two legs interact among themselves via the non-local interaction  $U_{AB}$ .

mapped to the spin systems under proper conditions, it promises a direct connection to the many-electron systems and magnetism [58]. One such recent studies on multi-component bosons in optical superlattices has predicted various gapped phases using the single site mean-field approximation where the bosons are assumed to be softcore in nature and the intra-species interactions are considered to be of identical strength [59]. As a result the influence of one species of atoms on the other and vice-versa is similar in nature.

At this point we consider a bilayer bosonic system in optical superlattice as depicted in Fig. 1(a). The construction of the bilayer system is in such a way that both the layers are identical to each other in terms of lattice translation and a two-period superlattice potential is present only along the  $x$ -direction. As a result, the lattice periodicity is doubled in the  $x$ -direction where as along the  $y$ -direction there is no change in the periodicity. In principle, one can consider the superlattice potential along both the directions which is expected to exhibit similar particle dynamics in both the directions. However, the choice made in this work provides a situation where the particles tend to localise in every alternate sites due to the superlattice potential along one direction where as they are free to move on the other direction. In such a system we consider the bosons in layer-A to be of softcore in nature where as bosons in layer-B experience two or three-body hardcore constraint. We assume the particles are of dipolar in nature in both the layers and there exists only inter-layer interactions and the intra-layer interactions are suppressed. This situation can be achieved by orienting the dipoles in such a way that they are at magic angles with the line joining two nearest neighbour dipoles along both  $x$ - and  $y$ -directions of the layer. In such a scenario, the angle made with the

line joining the dipoles sitting in two different layers are different from the magic angle resulting in a finite repulsive interaction which is proportional to  $(1 - 3\cos^2\theta)$  as depicted in Fig. 1(b).

The model which describes such system is the modified Bose-Hubbard model given as:

$$\begin{aligned}
 H = & -t \sum_{\langle i,j \rangle, \sigma \in [A, B]} (a_{i\sigma}^\dagger a_{j\sigma} + H.c.) \\
 & + \frac{U_\sigma}{2} \sum_{i, \sigma \in [A, B]} \left[ n_{i\sigma}(n_{i\sigma} - 1) - (\mu_\sigma - \lambda_i)n_{i\sigma} \right] \\
 & + U_{AB} \sum_i n_{iA} n_{iB}
 \end{aligned} \tag{1}$$

Here,  $a_{i\sigma}^\dagger (a_{i\sigma})$  is the creation (annihilation) operator which creates (destroys) a boson in layer  $\sigma (= A, B)$  and at site  $i$ ,  $n_{i\sigma} = a_{i\sigma}^\dagger a_{i\sigma}$  is the number operator and  $t$  is the hopping amplitude between any two nearest neighbour sites  $i$  and  $j$ . While  $U_\sigma$  represents the local two-body intra-layer interactions,  $U_{AB}$  represents the inter-layer two body interaction.  $\mu_\sigma$  is the chemical potential and  $\lambda_i$  is the superlattice potential along the  $x$ -direction which is  $0(\lambda)$  for odd(even) site indices as shown in Fig. 1(a). The two and three body constraints in layer-B are achieved by considering  $(a^\dagger)^2 = 0$  and  $(a^\dagger)^3 = 0$  respectively. Note that for the HCBs in layer-B,  $U_{\sigma=B} \rightarrow \infty$  and the terms associated to  $U_{\sigma=B}$  will vanish in model(1) due to the hardcore constraint.

The remaining part of the paper is organised as follows. In Sec. II, we give a brief discussion on the method used in this work. Section III contains the results and discussion of our work and we finally present the conclusion in Sec. IV.

## II. METHOD

We investigate the ground state properties of the model given in Eq. 1 by considering softcore bosons in layer-A whereas loading layer-B with HCBs and TBCs separately in two different scenarios. In both the cases we study the phase diagram of the system and obtain various gapped phases which appear at commensurate as well as incommensurate densities. We also show how the tip positions of these gapped phases or in other words the gapped to gapless phase transitions behave by changing the constraint on the bosons in layer-B. To this end we implement the cluster mean-field theory(CMFT) approach to analyse the Eq. 1. In the end we utilise the well known density matrix renormalization group (DMRG) method for the two-leg ladder model to examine the features in one dimension. It is to be noted that this problem can also be analysed using the simple mean-field decoupling approximation [60] which can capture the qualitative physics of the system. However, in order to achieve better accuracy we employ the CMFT approach. For the models like shown in Eq. 1, the CMFT method works

fairly well with less computational complexities and may approach the Quantum Monte Carlo results in the thermodynamic limit for some specific situations [22, 61, 62].

In the CMFT method the entire system is divided into identical clusters of limited number of sites which can be treated exactly and then the coupling between different clusters are treated in a mean-field way. The accuracy of this method improves by increasing the number of sites in the cluster. With this approximation the original Hamiltonian of Eq. 1 can be written as

$$H = H_C + H_{MF} \quad (2)$$

where  $H_C(H_{MF})$  is the cluster(mean-field) part of the Hamiltonian.  $H_C$  is same as Eq. 1 limited to the cluster size. The hoppings between the clusters are then approximated using the simple mean-field type decoupling scheme given as

$$a_{i\sigma}^\dagger a_{j\sigma} = \langle a_{i\sigma}^\dagger \rangle a_{j\sigma} + a_{i\sigma}^\dagger \langle a_{j\sigma} \rangle - \langle a_{i\sigma}^\dagger \rangle \langle a_{j\sigma} \rangle \quad (3)$$

Introducing the two layer-dependent SF order parameter  $\psi_{i\sigma} = \langle a_{i\sigma}^\dagger \rangle = \langle a_{i\sigma} \rangle$  and using Eq. 3 we write the  $H_{MF}$  as

$$H_{MF} = -t \sum_{\sigma, \langle i, j \rangle} [(a_{i\sigma}^\dagger + a_{i\sigma})\psi_{j\sigma} - \psi_{i\sigma}^* \psi_{j\sigma}] \quad (4)$$

In our calculation we have set  $t = 1$  to make all the physical quantities dimensionless. For the CMFT calculation we use a four sites cluster which consists of two sites from both the layers. We call this a supercell in the following discussion. We define the quantity

$$n = \sum_{\sigma \in [A, B]} \sum_{i=1}^2 n_{i\sigma} \text{ and } \rho = \frac{1}{4}n \text{ which are the total particle number and density in one supercell to distinguish various phases.}$$

We also assume equal chemical potentials for bosons in both the layers by making  $\mu_A = \mu_B = \mu$  in our calculation. By fixing the values of  $U_A, U_B$  (in case of TBCs) and  $U_{AB}$  we compute the complete phase diagram in the  $\mu$  vs  $\lambda$  plane. One can in principle fix the value of  $\lambda$  and vary the interactions as done in Ref. [59]. However, to understand the effect of the superlattice potential on the phase diagram, we consider a range of  $\lambda$  in our calculation. Further we analyse the system in one dimension by considering a two-leg ladder which can be viewed as two superlattice chains coupled via the dipole-dipole interaction. We study the model(1) by using the DMRG method by considering  $\sigma$  as the two legs of the ladder. In our DMRG calculation we assume system sizes up to 100 sites and 500 density matrix eigenstates. The cluster and system size considered in our calculation are found to be sufficient to capture the physics we are interested in.

### III. RESULTS AND DISCUSSION

#### A. Hardcore constraint for bosons in layer-B

In this part, we discuss the case when the bosons in layer-B are hardcore in nature. In the decoupled layer limit i.e.  $U_{AB} = 0$ , both the layers behave as independent two dimensional (2d) systems. It is well known that there exists a critical value of  $\lambda$  for which the system undergoes an SF to MI transitions at half filling for both hardcore and softcore bosons in 2d [10, 51, 63]. Therefore, it is expected that the first Mott lobe would appear in the system after a critical value of  $\lambda$  for density  $\rho = 1/4$  where any one of the layers attains half filling. At this stage the inter-layer interaction  $U_{AB}$  has no role on the phase diagram as the particles reside in any one of the layer. However, with the increase in the chemical potential  $\mu$  both the layers get populated and one may see interesting interplay between  $U_A, U_{AB}$  and  $\lambda$  which leads to various gapped phases and transitions to the SF phase at different integer and non integer fillings of individual layers as shown in Fig. 2. In this paper we call all the gapped phases the MI phases although the ones at non integer densities are different from the usual MI phase where each site is occupied with same integer number of bosons [47]. However, in the case of superlattices, one can consider the density with respect to the unit-cell (the periodicity of the superlattice) so that the gapped phases at non integer densities can be called as the MI phases for those particular densities.

The phase diagram of Fig. 2 is obtained by self consistently diagonalising the Hamiltonian shown in Eq. 2 to obtain the ground state wave function and then the superfluid order parameter  $\psi$  as discussed in the previous section. By considering a large onsite interaction  $U_A = 80$  and  $U_{AB} = U_A/2$  which is sufficient to establish various gapped phases for the softcore bosons in one layer

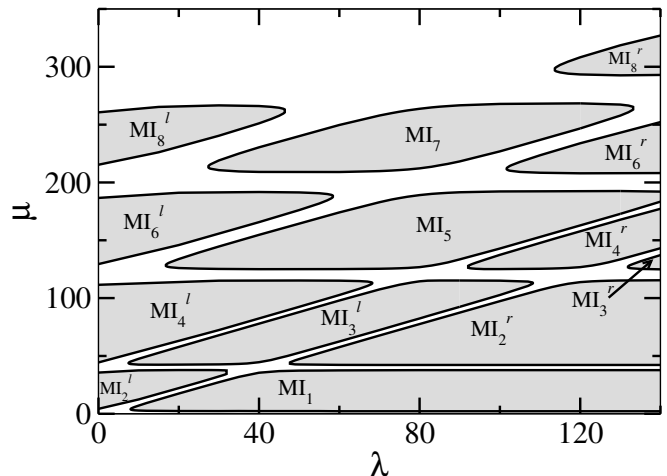


FIG. 2. CMFT phase diagram when bosons in layer-A are softcore and in layer-B are HCBs. Here  $U_A = 80$  and  $U_{AB} = 40$ .

TABLE I. Table depicting various MI states when atoms in layer-B are HCBs. Each state shows the density distribution in the supercell corresponding to a particular MI state for a given  $n$  and  $\rho$ .

Boson distribution in the unit cell		
$n$	$\rho$	Supercell Configuration
1	0.25	$MI_1 = \begin{vmatrix} 0 & 1 \\ 0 & 0 \end{vmatrix}$ or $MI_1 = \begin{vmatrix} 0 & 0 \\ 0 & 1 \end{vmatrix}$
2	0.5	$MI_2^I = \begin{vmatrix} 0 & 1 \\ 1 & 0 \end{vmatrix}$ or $MI_2^I = \begin{vmatrix} 1 & 0 \\ 0 & 1 \end{vmatrix}$ and $MI_2^I = \begin{vmatrix} 0 & 1 \\ 0 & 1 \end{vmatrix}$
3	0.75	$MI_3^I = \begin{vmatrix} 1 & 1 \\ 0 & 1 \end{vmatrix}$ and $MI_3^I = \begin{vmatrix} 0 & 2 \\ 0 & 1 \end{vmatrix}$
4	1.0	$MI_4^I = \begin{vmatrix} 1 & 1 \\ 1 & 1 \end{vmatrix}$ and $MI_4^I = \begin{vmatrix} 1 & 2 \\ 0 & 1 \end{vmatrix}$
5	1.25	$MI_5 = \begin{vmatrix} 1 & 2 \\ 1 & 1 \end{vmatrix}$
6	1.5	$MI_6^I = \begin{vmatrix} 2 & 2 \\ 1 & 1 \end{vmatrix}$ and $MI_6^I = \begin{vmatrix} 1 & 3 \\ 1 & 1 \end{vmatrix}$
7	1.75	$MI_7 = \begin{vmatrix} 2 & 3 \\ 1 & 1 \end{vmatrix}$
8	2.0	$MI_8^I = \begin{vmatrix} 3 & 3 \\ 1 & 1 \end{vmatrix}$ and $MI_8^I = \begin{vmatrix} 2 & 4 \\ 1 & 1 \end{vmatrix}$

and by varying  $\lambda$  for a wide range of values, we obtain the entire phase diagram which consists of the gapped MI lobes and the intermediate SF phases. Here we define the total superfluid order parameter  $\rho_s = \frac{1}{4} \sum_{i,\sigma} |\psi_{i\sigma}|^2$ , where  $\psi_{i\sigma}$  is the layer dependent superfluid order parameter as discussed in the previous section. The gapped phases are obtained by looking at the vanishing up of the total superfluid order parameter with respect to the chemical potential in the  $\rho_s$  vs  $\mu$  plot for several values of  $\lambda$ . In Fig. 3 we show  $\rho$  (solid blue line) and  $\rho_s$  (dashed green line) with respect to  $\mu$  for  $\lambda = 10, 70, 140$  which cut through the gapped phases in Fig. 2 parallel to the  $\mu$  axis. It can be seen that for a particular  $\lambda$ , as  $\mu$  increases the plateaus in  $\rho$  appear and at the same time  $\rho_s$  vanishes corresponding to the MI phases. We denote the MI phases as  $MI_n$  where the subscript  $n$  indicates the total number of particles i.e.  $n_A + n_B$  in a supercell. The possible supercell atom distribution for all the MI phases are presented in Table. I.

It can be seen from Fig. 2 that the first lobe which corresponds to the  $MI_1$  appears after a critical  $\lambda \sim 8$  at  $\rho = 1/4$  as discussed before. The gap continues to be finite and the lobe expands as  $\lambda$  increases further. Upon increasing the value of  $\mu$  or in other words by increasing the particle number in the system, the other gapped phases start to appear, which are seen as plateaus in the  $\rho$  vs  $\mu$  plot shown in Fig. 3. For total density  $\rho = 1/2$  (half filling of both the layers), there exists two gapped lobes separated by the SF phase as a function of  $\lambda$ . The appearance of large gap at vanishing  $\lambda$  can be attributed to the effect of  $U_{AB}$  which prevents the atoms in layer-A and layer-B to occupy the same sites. Hence, one may expect a gapped phase which is similar to the checker-board

solid for the Bose-Fermi mixture on a square lattice [64]. We call this phase as the  $MI_2^I$  phase. As discussed in Ref. [64], the stability of this gapped phase depends on the ratio  $U_{AB}/U_A$ . In our case  $U_{AB}/U_A = 0.5$ , which is sufficient to open a gap in the system. However, the gap gradually decreases as the value of  $\lambda$  increases and as a result the system enters into the SF phase. This is because of the increase in the effective onsite potential in every alternate sites on both the layers which results in a smaller ratio  $U_{AB}/U_A$ . Increasing in value of  $\lambda$  further, the gapped phase reappears after a critical  $\lambda \sim 47.6$ . At this stage, the superlattice potential is very strong compared to the ratio  $U_{AB}/U_A$  and the bosons reside in the deep lattice sites. We call this gapped phase the  $MI_2^I$  phase which is similar to the striped phase for the  $2d$  case. The density distribution can be seen from the  $\rho$  vs.  $\mu$  plot as shown in Fig. 3 (see figure for detail).

At this stage further increase in density results in the next gapped phases at  $\rho = 3/4$ . The situation at this density is completely different from the case of half density. Here we find that the system is initially in the gapless SF phase for a range of  $\lambda$  starting from  $\lambda = 0$  and there exists a gapped island for some intermediate range of  $\lambda$  and then a gapped phase for the large values of  $\lambda$ . The physics at this density can be understood by the following analysis. For  $\lambda = 0$ , as  $\mu$  increases the layer-A will start to get populated first due to the softcore nature

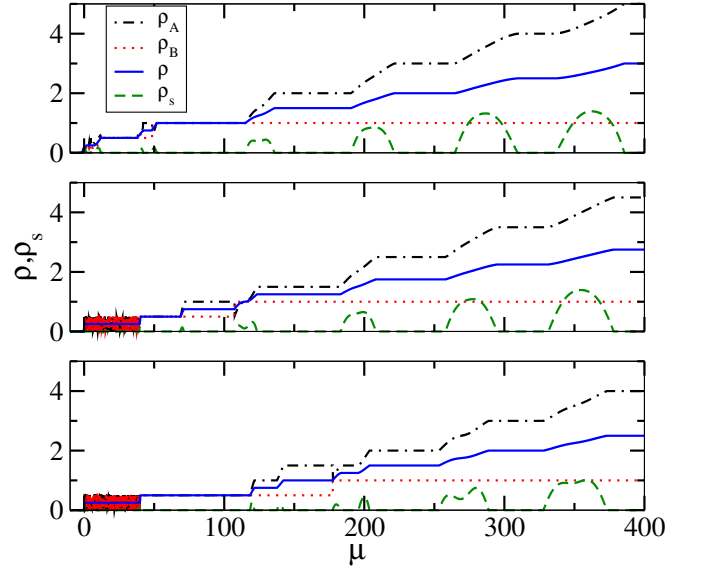


FIG. 3. (Color online) Variation of  $\rho$  (solid blue curve) and  $\rho_s$  (dashed green curve) with respect to  $\mu$  for  $\lambda = 10, 70, 140$  shows the gapped and gapless phases when layer-B has HCBs. The plateaus in  $\rho$  correspond to the gap in the MI phases whereas the shoulders around the plateaus (where the values of  $\rho_s$  are finite) indicate the gapless SF phase. We also plot the individual layer densities as  $\rho_A$  (dot dashed curve) and  $\rho_B$  (dotted curve) for clarity. Due to the hardcore nature  $\rho_B$  saturates at one. The fluctuations in  $\rho_A$  and  $\rho_B$  are due to the degenerate states in the CMFT calculation.



and all the sites are occupied by one atom each giving rise to unit filling and the layer-B remains at half filling. At unit filling the layer-A is in the MI phase as  $U_A$  is sufficiently strong. As a result, the atoms in layer-B will experience equal repulsion  $U_{AB}$  from all the sites of layer-A and hence they can move freely giving rise to the SF phase of layer-B. Therefore, the system as a whole is gapless although layer-A is in the MI state. The increase in  $\lambda$ , however, introduces the gap in the system by localising the hardcore bosons into the deep sites of layer-B while the layer-A remains in the MI phase. The resulting system is therefore, a gapped phase. This phase is called the  $MI_3^l$  phase which lies between  $\lambda \sim 7.5$  and  $\lambda \sim 108.4$ . Further increase in  $\lambda$  leads to increase in particle-hole fluctuation and the gapped MI phase starts to melt and the SF phase reappears in the system. Eventually, the system enters into another gapped phase after a critical value of  $\lambda \sim 131.10$  where in layer-A two bosons are localized in the deep lattice sites. We call this phase as the  $MI_3^r$  phase as depicted in the phase diagram of Fig. 2.

At this stage, further increase in the value of  $\mu$  will facilitate addition of bosons in layer-B which saturates at unit filling due to the hardcore nature of bosons where all the sites are occupied by one boson each. This situation corresponds to the  $MI_4$  phases in the phase diagram where the total density of the system is  $\rho = 1$ . When  $\lambda$  is small, we have every sites in both the layers occupied by one atom each and this phase is called the  $MI_4^l$ . When  $\lambda$  increases, the  $MI_4^l$  phase melts and the system enters into the SF phase and eventually leading to the  $MI_4^r$  phase where the atoms in layer-A occupy the deep sites while the layer-B maintains the uniform density due to the hardcore nature. In such a situation the layer-A is like the striped phase and layer-B is saturated. These features can be clearly seen from the individual layer densities as shown in Fig. 3.

Similar situation arises for the other integer and non-integer densities where two distinct gapped phases appear at two limits of the superlattice potential which are separated by the SF phase as depicted in the phase diagram of Fig. 2. The corresponding boson distributions are shown in Table.I for clarity. For quarter-integer densities, the gapped islands appear for a range of intermediate values of  $\lambda$  separated by the SF phase. It is to be noted that the tip of the right lobes shifts towards larger values of  $\lambda$  as  $\rho$  increases. However, there occurs an interesting pattern for the left lobes where the tip first shifts towards larger  $\lambda$  up to  $MI_4^l$  and then shifts left for higher densities. The appearance of this feature is attributed to the presence of bosons in layer-B in all the lattice sites after a critical density  $\rho \geq 1$ . At these densities, the bosons in layer-A does not get affected by the presence of the bosons in layer-B as it experiences uniform repulsion which is equal to  $U_{AB}$  from all sites. Therefore, the physics of the system is governed only by the properties of bosons in layer-A as discussed in Ref. [10]. The  $MI^l$ -SF transitions happens for smaller and smaller values of  $\lambda$  as the density increases because the increase in density leads

to the decrease in the effective onsite interactions on the shallow lattice sites. Therefore, the  $MI^l$  lobes melt into the SF phases due to the hopping  $t$  which dominates over the interactions. On the other hand the SF- $MI^r$  transition points shift towards the larger values of  $\lambda$  at higher densities because of the increase in number of particles in the deep wells which results in an increase in  $U_{AB}$ . Therefore, a stronger  $\lambda$  is necessary to introduce the  $MI^r$  phases as can be seen from the phase diagram.

### B. Three-body constraint for bosons in layer-B

Now we discuss the case in which we replace the bosons in layer-B with the TBCs. As discussed before, the effect of three-body constraint is a result of large three-body onsite repulsion i.e.  $W \rightarrow \infty$ . In such a situation the maximum number of bosons allowed per lattice site is two i.e.  $(a^\dagger)^3 = 0$ . Such constrained bosons may impart significant effects on the overall phase diagram of bosons in optical superlattice. Note that, in this case we have finite values of two-body interaction  $U_B$  in layer-B. similar to the previous section, we numerically solve the mean-field Hamiltonian given in Eq. 2 and with  $U_A = U_B = 80$  and  $U_{AB} = 40$  and varying  $\lambda$  we obtain various gapped phases. The ground state phase diagram is shown in Fig. 4 and the particle distributions are shown in Table-II.

In Fig. 5 we show  $\rho, \rho_s - \mu$  curves for  $\lambda = 10, 70, 140$  along the cuts through the gapped phases in Fig. 4. As discussed in the previous section we see that for a particular  $\lambda$ , as the chemical potential increases the plateaus in  $\rho$  appear and at the same time  $\rho_s$  vanishes which correspond to the MI phases which are explained in Table-II.

It can be seen that the phase diagram for this case exhibits distinct features along with some similarities com-

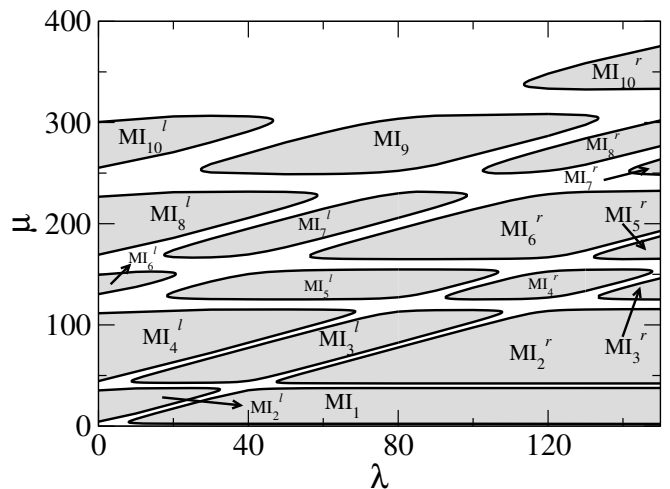


FIG. 4. CMFT phase diagram when bosons in layer-A are softcore and in layer-B are TBCs. Here  $U_A = U_B = 80$  and  $U_{AB} = 40$ .

pared to the one obtained when bosons in layer-B was hardcore in nature (compare with Fig. 2). Although the appearance of the MI phases for the odd (total) densities show similar behavior as the previous case, the even lobes exhibit different features with respect to their tip positions. It can be easily seen that the features in the part of the phase diagram from  $n = 6$  onwards matches well with the phase diagram of the previous case (when the layer-B was hardcore) except the first lobe at  $n = 1$  of Fig. 2. This can be understood as follows. Let's consider the  $\lambda = 0$  case for simplicity. As the layer-B is occupied by TBCs now, for  $n = 6$  the density of the supercell is 1.5. This means, there are two extra particles on top of the  $\rho = 1$  lobe ( $\text{MI}_4^l$ ). At  $\rho = 1$ , each sites of both the layers are occupied by one particle because of large onsite interactions  $U_A$  and  $U_B$ . Therefore, any extra particle which gets added to layer-B containing the TBCs will behave like hardcore bosons on top of the uniform particle distribution. Hence, the effective system becomes equivalent to the one considered in the previous section. However, there exists different gapped phases at low density regimes i.e. upto  $n = 6$  lobes. For  $n = 1$  ( $\rho = 0.25$ ) we get the  $\text{MI}_1$  phase which is similar to the one in Fig. 2 which starts after finite value of  $\lambda \sim 8$ . As the number of particles increases, the second gapped phase  $\text{MI}_2^l$  appears at  $n = 2$  ( $\rho = 0.5$ ) for  $\lambda = 0$  and this survives upto a critical value of  $\lambda \sim 32$  and after this the system

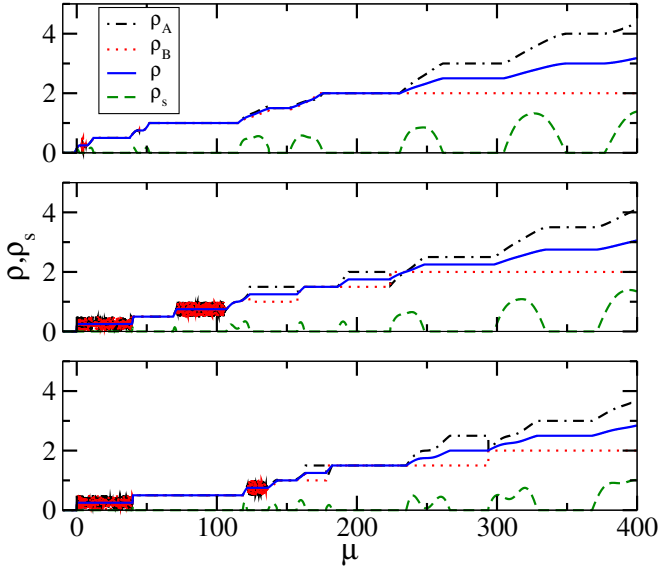


FIG. 5. (Color online) Figure shows the value of  $\rho$  (solid blue curve) and  $\rho_s$  (dashed green curve) with respect to  $\mu$  for  $\lambda = 10, 70, 140$  corresponding to the gapped and gapless phases when bosons in layer-B are TBCs. The plateaus in  $\rho$  indicates the gap in the MI phases whereas the shoulder around the plateaus (where the values of  $\rho_s$  are finite) correspond to the gapless SF phase. We also plot the individual layer densities as  $\rho_A$  (dot dashed curve) and  $\rho_B$  (dotted curve) for clarity. Note that  $\rho_B$  saturates at two after a certain chemical potential due to the three-body constraint.

TABLE II. Table depicting various MI states when atoms in layer-B are TBCs. Each state shows the density distribution in the supercell corresponding to a particular MI state for a given  $n$  and  $\rho$ .

Boson distribution in the unit cell		
n	$\rho$	Supercell Configuration
1	0.25	$\text{MI}_1 = \begin{vmatrix} 0 & 1 \\ 0 & 0 \end{vmatrix}$ or $\text{MI}_1 = \begin{vmatrix} 0 & 0 \\ 0 & 1 \end{vmatrix}$
2	0.5	$\text{MI}_2^l = \begin{vmatrix} 0 & 1 \\ 1 & 0 \end{vmatrix}$ or $\text{MI}_2^l = \begin{vmatrix} 1 & 0 \\ 0 & 1 \end{vmatrix}$ and $\text{MI}_2^s = \begin{vmatrix} 0 & 1 \\ 0 & 1 \end{vmatrix}$
3	0.75	$\text{MI}_3^l = \begin{vmatrix} 1 & 1 \\ 0 & 1 \end{vmatrix}$ or $\text{MI}_3^l = \begin{vmatrix} 0 & 1 \\ 1 & 1 \end{vmatrix}$ and $\text{MI}_3^s = \begin{vmatrix} 0 & 2 \\ 0 & 1 \end{vmatrix}$ or $\text{MI}_3^s = \begin{vmatrix} 0 & 1 \\ 0 & 2 \end{vmatrix}$
4	1.0	$\text{MI}_4^l = \begin{vmatrix} 1 & 1 \\ 1 & 1 \end{vmatrix}$ and $\text{MI}_4^r = \begin{vmatrix} 1 & 1 \\ 0 & 2 \end{vmatrix}$ or $\text{MI}_4^r = \begin{vmatrix} 0 & 2 \\ 1 & 1 \end{vmatrix}$
5	1.25	$\text{MI}_5^l = \begin{vmatrix} 1 & 2 \\ 1 & 1 \end{vmatrix}$ and $\text{MI}_5^s = \begin{vmatrix} 1 & 2 \\ 0 & 2 \end{vmatrix}$
6	1.5	$\text{MI}_6^l = \begin{vmatrix} 2 & 1 \\ 2 & 1 \end{vmatrix}$ or $\text{MI}_6^l = \begin{vmatrix} 1 & 2 \\ 1 & 2 \end{vmatrix}$ $\text{MI}_6^s = \begin{vmatrix} 2 & 1 \\ 1 & 2 \end{vmatrix}$ or $\text{MI}_6^s = \begin{vmatrix} 1 & 2 \\ 2 & 1 \end{vmatrix}$ and $\text{MI}_6^s = \begin{vmatrix} 1 & 2 \\ 1 & 2 \end{vmatrix}$
7	1.75	$\text{MI}_7^l = \begin{vmatrix} 2 & 2 \\ 1 & 2 \end{vmatrix}$ and $\text{MI}_7^r = \begin{vmatrix} 1 & 3 \\ 1 & 2 \end{vmatrix}$
8	2.0	$\text{MI}_8^l = \begin{vmatrix} 2 & 2 \\ 2 & 2 \end{vmatrix}$ and $\text{MI}_8^s = \begin{vmatrix} 1 & 3 \\ 2 & 2 \end{vmatrix}$
9	2.25	$\text{MI}_9 = \begin{vmatrix} 2 & 3 \\ 2 & 2 \end{vmatrix}$
10	2.5	$\text{MI}_{10}^l = \begin{vmatrix} 3 & 3 \\ 2 & 2 \end{vmatrix}$ and $\text{MI}_{10}^s = \begin{vmatrix} 2 & 4 \\ 2 & 2 \end{vmatrix}$

becomes gapless. In this case, each layer is occupied by one boson. Further increase in  $\lambda$  leads to the  $\text{MI}_2^r$  phase, where the particles live in the deep sites. Similarly, the  $\text{MI}_4$  phases appear for  $n = 4$  ( $\rho = 1$ ) in the beginning when  $\lambda = 0$  and the system is a proper Mott insulator at unit filling. Increase in  $\lambda$  will melt the gap and the SF phase appears and further increase in  $\lambda$  will re-introduce the gap and the system gets into the  $\text{MI}_4^r$  phase. In this phase, there can be two possible particle distributions in the lattice where two particles populate the deep sites of layer-A while sites of layer-B are uniformly filled by one particle in each site and vice-versa. This gapped phase vanishes at  $\lambda \sim 148$  and further increase in  $\lambda$  may lead to another gapped phase where the deep sites of both the layers will be occupied by two particles (not in the range of  $\lambda$  considered here). The physics of odd integer lobes can also be understood from the similar analogies discussed above.

### C. Phase diagram in one dimension

In this section we complement our CMFT results presented above by analyzing the situation in one dimension.

sion. The one dimensional analogue of bilayer geometry is a two-leg ladder where the layer-A(B) is replaced by leg-A(B) as shown in Fig. 1(c). The one dimensional ladder geometries are extremely important in the context of condensed matter systems as it resembles to several structures of compounds of interest. The ladder geometries has been discussed in great detail in terms of Hubbard model [65–77] and Bose-Hubbard model [21, 78–82]. Analogous to the 2d case we assume only inter-leg dipole-dipole interactions by aligning the dipoles at magic angle with each other along the leg direction. The physics of this system will be similar to the two dimensional case due to the construction of the bilayer lattice in our case as discussed earlier. We employ the DMRG method to solve the model(Eq. 1) in the canonical ensemble to compute the ground state energy and wave function. To separate the gapped and gapless regions we calculate the single particle gap which is defined as

$$G_L = \mu^+ - \mu^-, \quad (5)$$

with  $\mu^+ = E_L(N+1) - E_L(N)$  and  $\mu^- = E_L(N) - E_L(N-1)$  are the chemical potentials and  $E_L(N)$  is the the ground state energy of a system of length  $L$  and  $N = N_A + N_B$  is the total number of particles in the system. We obtain the ground state phase diagram for both the cases with bosons of leg-B separately being HCBs and TBCs while bosons in leg-A are softcore in nature which are shown in Fig. 6( $U_A = 20$  and  $U_{AB} = 10$ ) and Fig. 7( $U_{A,B} = 20$  and  $U_{AB} = 10$ ) respectively. One can easily see that the phase diagrams of Fig. 6 and Fig. 7 qualitatively match fairly well with the ones obtained using the CMFT method i.e. Fig. 2 and Fig. 4 respectively. When bosons in leg-B are HCBs, we observe the MI tip positions first increase and then decrease as shown in Fig. 6 while there is an alternating increase and decrease of the tip positions when the bosons in leg-B are TBCs as plotted in Fig. 7. The boundaries of the MI lobes are computed by extrapolating the  $\mu$  values across

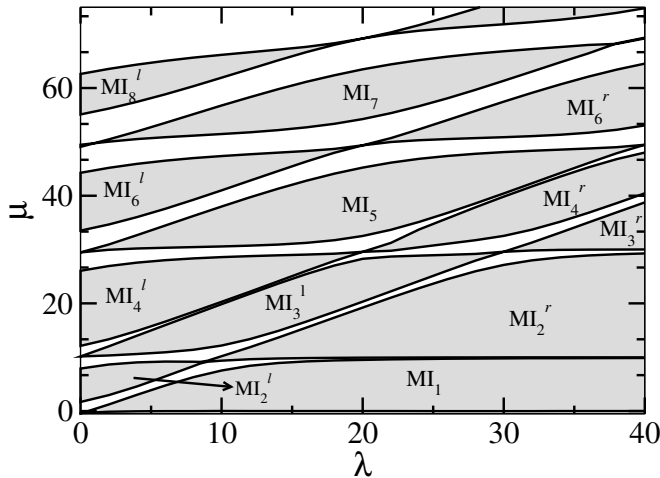


FIG. 6. DMRG phase diagram when bosons in leg-A are softcore in nature and bosons in leg-B are HCBs.

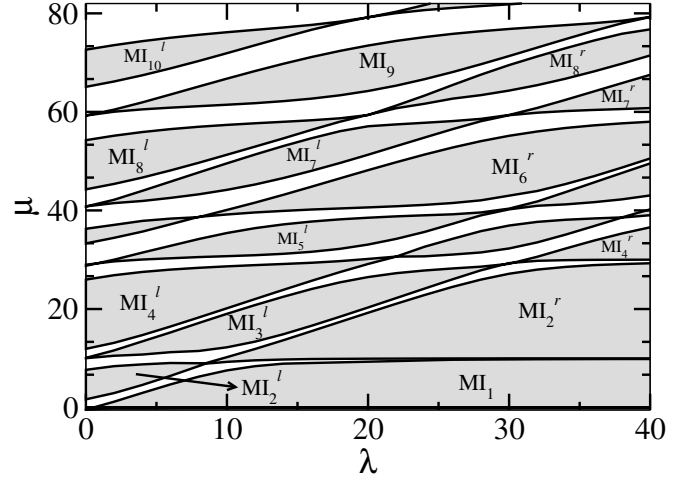


FIG. 7. DMRG phase diagram when bosons in leg-A are softcore in nature and bosons in leg-B are TBCs.

the MI plateaus to thermodynamic limit by quadratic fitting. In Fig. 8, we show the finite size extrapolation of  $\mu^+$  (dashed) and  $\mu^-$  (solid) for  $\lambda = 18, 20, 22, 24$  and 26. This clearly shows that  $G_{L \rightarrow \infty}$  remains finite in the gapped phase and vanishes in the gapless region which clearly distinguish between the gapped and gapless phases in the phase diagrams.

Further, to understand the particle distribution in real space we compute the expectation value of the number operator as

$$\langle n_i \rangle = \langle \Psi_0 | n_i | \Psi_0 \rangle \quad (6)$$

where  $|\Psi_0\rangle$  is the ground state wave function of the system. As an example, in Fig. 9 we plot  $\langle n_i \rangle$  w.r.t. site index  $i$  for  $\lambda = 12$ (top) and  $\lambda = 28$ (bottom) correspond-

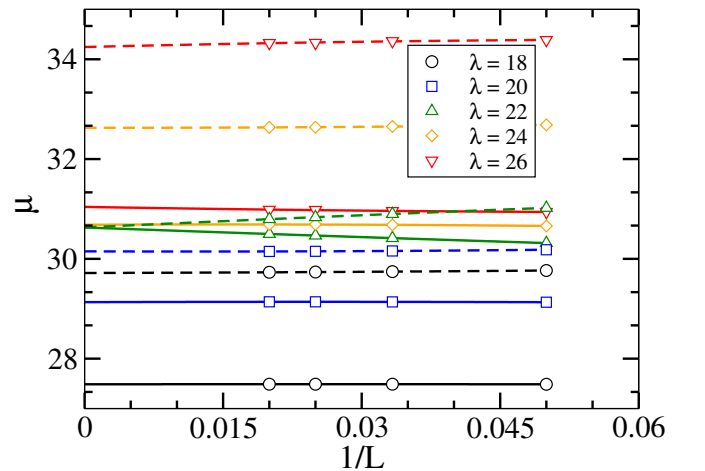


FIG. 8. (Color online) Finite size scaling of chemical potentials for  $\rho = 1.5$  for different values of  $\lambda$  corresponding to the phase diagram of Fig. 6 when bosons in leg-A are softcore in nature and bosons in leg-B are HCBs. The solid and dashed lines represent the fitted functions to  $\mu^+$  and  $\mu^-$  respectively.

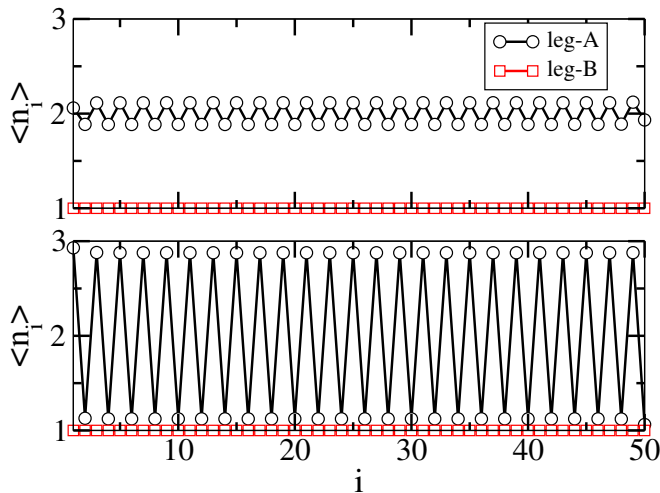


FIG. 9. (Color online) Density distribution of the system when  $\lambda = 12$ (top) and  $\lambda = 28$ (bottom) for  $\rho = 1.5$  corresponding to the phase diagram of Fig. 6. The black circles and red squares represent the density distribution of leg-A and leg-B respectively.

ing to the  $MI_6^l$  and  $MI_6^r$  phases respectively of the phase diagram shown in Fig. 6. It can be clearly seen that for  $\lambda = 12$  the leg-B is occupied by one hardcore boson in each site whereas in leg-A, each site is occupied by two atoms. However, for  $\lambda = 28$ , the leg-B is unaffected and leg-A shows  $|\dots 3\ 1\ 3\ 1\dots\rangle$  type of distribution corresponding to the  $MI_6^r$  phase. A similar  $\langle n_i \rangle$  vs  $i$  plot is shown in Fig. 10 for the  $MI_7$  phase of Fig. 7. Here we consider  $\lambda = 22$ (top) and  $38$ (bottom) which fall in two regions of the  $MI_7^l$  and  $MI_7^r$  phases respectively. For  $\lambda = 22$ , all the sites of leg-A are occupied by two particles each whereas

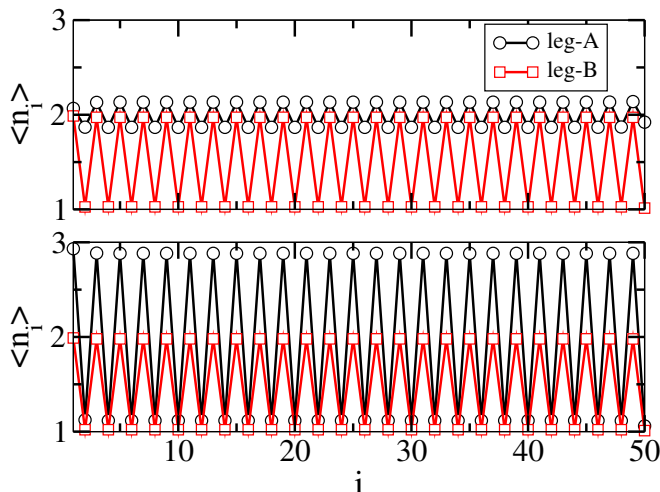


FIG. 10. (Color online) Density distribution of the system when  $\lambda = 22$ (top) and  $\lambda = 38$ (bottom) for  $\rho = 1.75$  corresponding to the phase diagram of Fig. 7. The black circles and red squares represent the density distribution of leg-A and leg-B respectively.

leg-B exhibits a finite density oscillation corresponding to  $|\dots 2\ 1\ 2\ 1\dots\rangle$  type of distribution. However, for large  $\lambda = 38$ , the density distribution of leg-A becomes  $|\dots 3\ 1\ 3\ 1\dots\rangle$  while the leg-B remains unaffected. It is to be noted that for the parameters considered here, the gapless regions between two gapped phases are very small compared to ones obtained using the CMFT method.

#### IV. CONCLUSION

We analyse the ground state properties of a system of interacting bosons in bilayer superlattice with inter-layer repulsion which can be introduced by the dipole-dipole interactions. Considering the bosons in one layer as softcore in nature and separately allowing two and three-body hardcore constraints in the other layer we obtain the ground state phase diagram using the CMFT approach. The phase diagrams exhibit various gapped MI phases at integer and half-integer densities. Due to the competition between the superlattice potential, intra- and inter-layer interactions and the constraints on the bosons of layer-B leads to interesting features in the phase diagram. It is shown that within the range of  $\lambda$  considered, we obtain two types MI lobes( $MI_n^l$  and  $MI_n^r$ ) separated by the SF region for a particular total number of particles in the supercell equal to  $n$ . Interestingly, when the hardcore constraint is applied in one layer, the tips of the  $MI_n^l$  lobes first shift towards higher values of  $\lambda$  and then gradually recede to the lower values of  $\lambda$ . At the same time the tips of the  $MI_n^r$  lobes shift towards the higher  $\lambda$  values with increase in density of the system. The situation is completely different when the three-body constraint is considered in one layer. The tips of MI lobes first oscillate and then after a critical density follows the trend similar to the one for the hardcore constraint. We further complement our findings by repeating the calculations in an one dimensional non-locally coupled ladder superlattice using the DMRG method and show that the quantum phase diagrams qualitatively agree with the CMFT method. The physics obtained in this work deals with the system of bosons in two-layer systems with different types of on-site interactions in a superlattice. The results provide detailed analysis of the effect of constrained bosons on the overall phase diagram of the bilayer system which is also equivalent to a two-component atomic systems. With the experimental progress in controlling local and dipole-dipole interactions in recent years, these findings can be experimentally observed with the existing quantum gas setups.

#### V. ACKNOWLEDGEMENT

We thank B. P. Das for useful discussion. The computational works were carried out using the Param-Ishan HPC facility at the Indian Institute of Tech-



nology - Guwahati, India. T.M. acknowledges DST-SERB for the early career grant through Project No.

ECR/2017/001069 and the hospitality received from ICTS-TIFR, Bangalore where part of the manuscript was written.

- 
- [1] M. Greiner, O. Mandel, T. Esslinger, T. W. Hänsch, and I. Bloch, *Nature* **415**, 39 EP (2002), article.
  - [2] M. P. A. Fisher, P. B. Weichman, G. Grinstein, and D. S. Fisher, *Phys. Rev. B* **40**, 546 (1989).
  - [3] D. Jaksch, C. Bruder, J. I. Cirac, C. W. Gardiner, and P. Zoller, *Phys. Rev. Lett.* **81**, 3108 (1998).
  - [4] S. Will, T. Best, U. Schneider, L. Hackermüller, D.S. Lühmann, and I. Bloch, *Nature* **465**, 197 (2010).
  - [5] M. J. Mark, E. Haller, K. Lauber, J. G. Danzl, A. J. Daley, and H.-C. Nägerl, *Phys. Rev. Lett.* **107**, 175301 (2011).
  - [6] A. J. Daley and J. Simon, *Phys. Rev. A* **89**, 053619 (2014).
  - [7] P. R. Johnson, E. Tiesinga, J. V. Porto, and C. J. Williams, *New Journal of Physics* **11**, 093022 (2009).
  - [8] D. S. Petrov, *Phys. Rev. Lett.* **112**, 103201 (2014).
  - [9] D. S. Petrov, *Phys. Rev. A* **90**, 021601 (2014).
  - [10] M. Singh, A. Dhar, T. Mishra, R. V. Pai, and B. P. Das, *Phys. Rev. A* **85**, 051604 (2012).
  - [11] T. Sowiński, R. W. Chhajlany, O. Dutta, L. Tagliacozzo, and M. Lewenstein, *Phys. Rev. A* **92**, 043615 (2015).
  - [12] A. J. Daley, J. M. Taylor, S. Diehl, M. Baranov, and P. Zoller, *Phys. Rev. Lett.* **102**, 040402 (2009).
  - [13] B. Paredes, A. Widera, V. Murg, O. Mandel, S. Fölling, I. Cirac, G. V. Shlyapnikov, T. W. Hänsch, and I. Bloch, *Nature* **429**, 277 (2004).
  - [14] M. A. Baranov, M. Dalmonte, G. Pupillo, and P. Zoller, *Chemical Reviews* **112**, 5012 (2012).
  - [15] S. Baier, M. J. Mark, D. Petter, K. Aikawa, L. Chomaz, Z. Cai, M. Baranov, P. Zoller, and F. Ferlaino, *Science* **352**, 201 (2016).
  - [16] L. Chomaz, D. Petter, P. Ilzhöfer, G. Natale, A. Trautmann, C. Politi, G. Durastante, R. M. W. van Bijnen, A. Patscheider, M. Sohmen, M. J. Mark, and F. Ferlaino, *Phys. Rev. X* **9**, 021012 (2019).
  - [17] L. Tanzi, E. Lucioni, F. Famà, J. Catani, A. Fioretti, C. Gabbanini, R. N. Bisset, L. Santos, and G. Modugno, *Phys. Rev. Lett.* **122**, 130405 (2019).
  - [18] F. Böttcher, J.-N. Schmidt, M. Wenzel, J. Hertkorn, M. Guo, T. Langen, and T. Pfau, *Phys. Rev. X* **9**, 011051 (2019).
  - [19] C. Trefzger, C. Menotti, and M. Lewenstein, *Phys. Rev. Lett.* **103**, 035304 (2009).
  - [20] A. Safavi-Naini, S. G. Söyler, G. Pupillo, H. R. Sadeghpour, and B. Capogrosso-Sansone, *Phys. Rev. Lett.* **15**, 013036 (2013).
  - [21] A. Argüelles and L. Santos, *Phys. Rev. A* **75**, 053613 (2007).
  - [22] M. Singh, S. Mondal, B. K. Sahoo, and T. Mishra, *Phys. Rev. A* **96**, 053604 (2017).
  - [23] J. Catani, L. De Sarlo, G. Barontini, F. Minardi, and M. Inguscio, *Phys. Rev. A* **77**, 011603 (2008).
  - [24] D. S. Hall, M. R. Matthews, J. R. Ensher, C. E. Wieman, and E. A. Cornell, *Phys. Rev. Lett.* **81**, 1539 (1998).
  - [25] J. Catani, L. De Sarlo, G. Barontini, F. Minardi, and M. Inguscio, *Phys. Rev. A* **77**, 011603 (2008).
  - [26] S. Trotzky, P. Cheinet, S. Fölling, M. Feld, U. Schnorrberger, A. M. Rey, A. Polkovnikov, E. A. Demler, M. D. Lukin, and I. Bloch, *Science* **319**, 295 (2008).
  - [27] R. Jördens, N. Strohmaier, K. Günter, H. Moritz, and T. Esslinger, *Nature* **455**, 204 (2008).
  - [28] A.-C. Voigt, M. Taglieber, L. Costa, T. Aoki, W. Wieser, T. W. Hänsch, and K. Dieckmann, *Phys. Rev. Lett.* **102**, 020405 (2009).
  - [29] M. Snoek, I. Titvinidze, I. Bloch, and W. Hofstetter, *Phys. Rev. Lett.* **106**, 155301 (2011).
  - [30] K. Günter, T. Stöferle, H. Moritz, M. Köhl, and T. Esslinger, *Phys. Rev. Lett.* **96**, 180402 (2006).
  - [31] G. Roati, F. Riboli, G. Modugno, and M. Inguscio, *Phys. Rev. Lett.* **89**, 150403 (2002).
  - [32] T. Best, S. Will, U. Schneider, L. Hackermüller, D. van Oosten, I. Bloch, and D.-S. Lühmann, *Phys. Rev. Lett.* **102**, 030408 (2009).
  - [33] L. He, Y. Li, E. Altman, and W. Hofstetter, *Phys. Rev. A* **86**, 043620 (2012).
  - [34] F. Hébert, G. G. Batrouni, X. Roy, and V. G. Rousseau, *Phys. Rev. B* **78**, 184505 (2008).
  - [35] T. Mishra, R. V. Pai, and B. P. Das, *Phys. Rev. A* **76**, 013604 (2007).
  - [36] T. Mishra, B. K. Sahoo, and R. V. Pai, *Phys. Rev. A* **78**, 013632 (2008).
  - [37] T. Ozaki and T. Nikuni, *Journal of the Physical Society of Japan* **81**, 024001 (2012).
  - [38] H. Pu and N. P. Bigelow, *Phys. Rev. Lett.* **80**, 1130 (1998).
  - [39] A. Kuklov, N. Prokof'ev, and B. Svistunov, *Phys. Rev. Lett.* **92**, 050402 (2004).
  - [40] L. Mathey, *Phys. Rev. B* **75**, 144510 (2007).
  - [41] A. Isacsson, M.-C. Cha, K. Sengupta, and S. M. Girvin, *Phys. Rev. B* **72**, 184507 (2005).
  - [42] S. Sugawa, K. Inaba, S. Taie, R. Yamazaki, M. Yamashita, and Y. Takahashi, *Nature Physics* **7**, 642 (2011).
  - [43] H. Hara, H. Konishi, S. Nakajima, Y. Takasu, and Y. Takahashi, *Journal of the Physical Society of Japan* **83**, 014003 (2014).
  - [44] S. Peil, J. V. Porto, B. L. Tolra, J. M. Obrecht, B. E. King, M. Subbotin, S. L. Rolston, and W. D. Phillips, *Phys. Rev. A* **67**, 051603 (2003).
  - [45] J. Sebby-Strabley, M. Anderlini, P. S. Jessen, and J. V. Porto, *Phys. Rev. A* **73**, 033605 (2006).
  - [46] M. Singh, A. Dhar, T. Mishra, R. V. Pai, and B. P. Das, *Phys. Rev. A* **85**, 051604 (2012).
  - [47] M. Singh and T. Mishra, *Phys. Rev. A* **94**, 063610 (2016).
  - [48] A. Dhar, T. Mishra, R. V. Pai, and B. P. Das, *Phys. Rev. A* **83**, 053621 (2011).
  - [49] A. Dhar, M. Singh, R. V. Pai, and B. P. Das, *Phys. Rev. A* **84**, 033631 (2011).
  - [50] A. Dhar, T. Mishra, R. V. Pai, S. Mukerjee, and B. P. Das, *Phys. Rev. A* **88**, 053625 (2013).
  - [51] R. Roth and K. Burnett, *Phys. Rev. A* **68**, 023604 (2003).
  - [52] F. Schmitt, M. Hild, and R. Roth, *Phys. Rev. A* **80**, 023621 (2009).

- [53] G. Roux, T. Barthel, I. P. McCulloch, C. Kollath, U. Schollwöck, and T. Giamarchi, *Phys. Rev. A* **78**, 023628 (2008).
- [54] J. Sebby-Strabley, M. Anderlini, P. S. Jessen, and J. V. Porto, *Phys. Rev. A* **73**, 033605 (2006).
- [55] P. Cheinet, S. Trotzky, M. Feld, U. Schnorrberger, M. Moreno-Cardoner, S. Fölling, and I. Bloch, *Phys. Rev. Lett.* **101**, 090404 (2008).
- [56] F. Grusdt, M. Hönig, and M. Fleischhauer, *Phys. Rev. Lett.* **110**, 260405 (2013).
- [57] S. Nascimbène, Y.-A. Chen, M. Atala, M. Aidelsburger, S. Trotzky, B. Paredes, and I. Bloch, *Phys. Rev. Lett.* **108**, 205301 (2012).
- [58] E. Altman, W. Hofstetter, E. Demler, and M. D. Lukin, *New Journal of Physics* **5**, 113a–113 (2003).
- [59] B.-L. Chen, S.-P. Kou, Y. Zhang, and S. Chen, *Phys. Rev. A* **81**, 053608 (2010).
- [60] K. Sheshadri, H. Krishnamurthy, R. Pandit, and T. Ramakrishnan, *EPL (Europhysics Letters)* **22**, 257 (1993).
- [61] I. Danshita, J. E. Williams, C. A. R. Sá de Melo, and C. W. Clark, *Phys. Rev. A* **76**, 043606 (2007).
- [62] Y.-C. Chen and M.-F. Yang, *Journal of Physics Communications* **1**, 035009 (2017).
- [63] B. Yang, H.-N. Dai, H. Sun, A. Reingruber, Z.-S. Yuan, and J.-W. Pan, *Phys. Rev. A* **96**, 011602 (2017).
- [64] M. Lewenstein, L. Santos, M. A. Baranov, and H. Fehrmann, *Phys. Rev. Lett.* **92**, 050401 (2004).
- [65] P. Donohue, M. Tsuchiizu, T. Giamarchi, and Y. Suzumura, *Phys. Rev. B* **63**, 045121 (2001).
- [66] A. E. Feiguin and M. P. A. Fisher, *Phys. Rev. B* **83**, 115104 (2011).
- [67] F. m. c. Crépin, N. Laflorencie, G. Roux, and P. Simon, *Phys. Rev. B* **84**, 054517 (2011).
- [68] M. Okumura, S. Yamada, M. Machida, and H. Aoki, *Phys. Rev. A* **83**, 031606 (2011).
- [69] C. Degli Esposti Boschi, A. Montorsi, and M. Roncaglia, *Phys. Rev. B* **94**, 085119 (2016).
- [70] W.-L. Liu, T.-Z. Yuan, Z. Lin, and W. Yan, *Chinese Physics B* **28**, 020303 (2019).
- [71] T. Giamarchi, *Quantum physics in one dimension*, Vol. 121 (Clarendon press, 2003).
- [72] M. Fabrizio, *Phys. Rev. B* **48**, 15838 (1993).
- [73] N. Nagaosa, *Solid State Communications* **94**, 495 (1995).
- [74] H. J. Schulz, *Phys. Rev. B* **53**, R2959 (1996).
- [75] L. Balents and M. P. A. Fisher, *Phys. Rev. B* **53**, 12133 (1996).
- [76] R. M. Noack, S. R. White, and D. J. Scalapino, *Physica C: Superconductivity* **270**, 281 (1996).
- [77] S. R. White, I. Affleck, and D. J. Scalapino, *Phys. Rev. B* **65**, 165122 (2002).
- [78] P. Donohue and T. Giamarchi, *Phys. Rev. B* **63**, 180508 (2001).
- [79] M. S. Luthra, T. Mishra, R. V. Pai, and B. P. Das, *Phys. Rev. B* **78**, 165104 (2008).
- [80] M. Singh, T. Mishra, R. V. Pai, and B. P. Das, *Phys. Rev. A* **90**, 013625 (2014).
- [81] P. Donohue and T. Giamarchi, *Phys. Rev. B* **63**, 180508 (2001).
- [82] M. A. Cazalilla, A. F. Ho, and T. Giamarchi, *Phys. Rev. B* **8**, 158 (2006).